MDPI

Review

57Fe Mössbauer Analysis of Meteorites and Tektites

Benilde F. O. Costa [1],*, Eduardo Ivo Alves [2], Pedro A. O. C. Silva [3] and António C. Batista [1]

1 University of Coimbra, Physics Department, CFisUC, P-3004-516 Coimbra, Portugal; castanhola@uc.pt
2 University of Coimbra, Department of Earth Sciences, CITEUC, P-3030-790 Coimbra, Portugal; e.ivo.alves@gmail.com
3 University of Coimbra, Physics Department, LIBPhys, P-3004-516 Coimbra, Portugal; pesilva@uc.pt
* Correspondence: benilde@uc.pt; Tel.: +35-12-3941-0630

Abstract: This review presents studies on iron meteorites (Campo del Cielo fall and an unregistered iron meteorite), an unregistered stony meteorite from Northwest Africa, and 13 tektites from the American, European, and Australasian strewn fields. The main experimental technique used in the studies was Mössbauer spectroscopy, both in transmission and backscattering geometries. For the latter, a MIMOS II spectrometer was used. Additionally, optical and scanning electron microscopies and X-ray diffraction were used. In the studied iron meteorites, kamacite is found as the main mineral. Campo del Cielo meteorite exhibits Widmanstätten patterns and schreibersite inclusions. The unregistered iron meteorite has Neumann lines and schreibersite inclusions. We have assigned Campo del Cielo as an octahedrite and the unregistered iron meteorite as a hexahedrite. The unregistered stony meteorite is composed mainly of iron-free silicates; at 4.2 K, the spectrum indicates maghemite and 1% troilite. The Cambodian tektite appeared individualized from other australasites, unlike the moldavite, which tends to cluster with them. Our analyses do not allow dismissing doubts on the provenance of tibetanites. The Fe^{3+}/Fe^{2+} ratio was found to be higher for Muong Nong-type tektites than for splash-form tektites, as expected from their morphology and solidification from melt at lower temperature.

Keywords: meteorites; tektites; Mössbauer spectroscopy

1. Introduction

Meteorites are bodies originating from outer space that survive their passage through the atmosphere. Their study is important: some of them, namely undifferentiated ones, contain more primitive materials for study of the Solar System and, being on Earth, they can be studied with a variety of techniques, from simple ones to more sophisticated ones. Roughly, meteorites can be divided into three large categories in terms of their structure and composition. Stony meteorites are rocks mainly composed of silicates. Stony-iron meteorites contain approximately equal amounts of metallic and stony materials. Iron meteorites are composed mainly of iron–nickel alloys. Structurally, iron meteorites can be divided in three groups: octahedrites, hexahedrites, and ataxites. Octahedrites are the only ones displaying Widmanstätten patterns [1]. They have between 6 and 16 wt.% Ni. Ataxites are a very rare class of iron meteorites. They do not exhibit a Widmanstätten structure and have 16 wt.% Ni or more. Hexahedrites have a Ni content below 6 wt.%.

Stony meteorites are the most common type of collected meteorites. Their name recalls the fact that they are mainly composed of silicate minerals (pyroxenes, olivines, and plagioclases) but often contain minor amounts of minerals, such as kamacite, α-Fe(Ni,Co), taenite, γ-Fe(Ni,Co), and other minor metallic minerals, such as Fe and/or Ni sulfides, oxides, and hydroxides. Stony meteorites can be subdivided in two sub-classes: chondrites, the most frequent, which contain millimeter-sized silicate (mainly olivine and pyroxene) spherules called chondrules, and achondrites, which lack chondrules. Being visually similar to basic igneous rocks, achondrites may often not be identified as meteorites; this

makes it difficult to evaluate their true proportion in the stony meteorites class, especially on collection sites with outcropping basic igneous rocks; conversely, meteorites collected on Antarctic ice can generally be well identified [2].

On the other hand, there are interesting natural glasses all related to meteorites and their impacts. Glasses are sometimes found in rocky meteorites as inclusions in minerals, mesostasis, pockets, or veins. These glasses have been identified either as residual liquids from which the associated minerals crystallized, as in terrestrial volcanism or, more recently, as an independent "primordial" phase [3]. At the site of a meteorite impact the so-called impactites may form. Impactites show characteristic breccia textures and very specific structures, such as shatter cones, and mineralogies, namely high-pressure and/or temperature silica polymorphs (tridimite, cristobalite, coesite, stishovite), and also glass. The volume and composition of impact glasses is dependent on the compositions of the impacted ground and the impactor meteorite, and on the dynamic characteristics of the impact. Impactites have been tentatively identified on Mars [4]. The volume of the produced impact melt can be orders of magnitude larger than the volume of the impactor meteorite itself [5]; part of this melt quenches in situ forming the above-mentioned impact glass and the remaining is ejected away, sometimes to large distances (thousands of kilometers), rapidly cooling while in flight.

Tektites are the natural glasses originated from fused material spilt during a meteorite impact [6]. Tektites are spread over several vast strewn fields on the Earth's surface. Four strewn fields have been well-established: moldavites in Europe, in the Czech Republic (the only ones that are light-green and translucent); bediasites and georgiaites in North America (Texas and Georgia, respectively); ivorites in Ivory Coast; indochinites, rizalites (from the Philippines), and australites, in the largest strewn field, which ranges from South Asia to the Antarctic Ocean [7]. Enclosed in the Australasian tektites strewn field lies a field of impact glasses, about 400 km^2 in area, on the Tasmanian West Coast, where the so-called Darwin glasses are found [8]. Thought to have been originated at the impact that produced Darwin crater, about 26 km south of Queenstown, Darwin glasses are macroscopically similar to moldavites—many samples are even translucent light-green, though not the one in this study, which is black—and were considered chemically indistinguishable from them [9].

Increasing interest on tektites has prompted more findings that are not easily attributed to the "classic" four strewn fields. Dunlap [10] published the first Mössbauer analyses of a Tibetan tektite, which are consistent with those of indochinites from Cambodia. Devouard et al. [11] identify a potentially new tektite (atacamaite) strewn field around the Atacama Desert, Chile, although later work [12] indicates this may be an impact-glass strewn field. Povenmire and Cornec [13] postulate another new strewn field in and around Belize.

Apart from the microtektites found in deep-sea sediments, tektites on land can be subdivided into three groups according to their geometry: splash-form tektites, aerodynamically ablated tektites, and Muong Nong-type tektites (with irregular shapes and a layered structure). Some authors suggested that Muong Nong-type tektites probably have not travelled far from their location of origin and may, therefore, be the closest to the original impact crater [14,15].

Mössbauer spectroscopy has its importance in the study of meteorites as it makes it possible to obtain information about iron-containing minerals. In the case of tektites, the knowledge of Fe^{3+}/Fe^{2+} ratios can provide information about their formation. The melting of crystalline rocks by a meteorite impact leads to a very unbalanced melting of silicates. The redox reactions that lead to equilibrium are mainly a function of temperature and fugacity of oxygen imposed on the melt but are also a function of the chemical composition of the melt itself. Mössbauer spectroscopy is one of the most powerful methods for determination of the iron atoms valence/spin state and coordination [16,17]. Amongst the advantages of Mössbauer spectroscopy when compared to other techniques are: (a) the small amount of sample required, (b) both ferric and ferrous ions are determined simultaneously, with no need for a separate analysis of the total iron, and (c) the Fe^{3+}/Fe^{2+}

ratio of a glass phase is determined independently of crystals that may also be present in the sample.

Tektites have a low Fe^{3+}/Fe^{2+} ratio [18] when compared with values of other silicate glasses, suggesting that they solidify in a low-oxygen environment. Muong Nong tektites have a higher Fe^{3+}/Fe^{2+} ratio than splash-form tektites, this being consistent with their morphology and the common idea that they solidify from melt at lower temperatures [19].

The oxygen partial pressure is an important factor in determining the Fe^{3+}/Fe^{2+} ratio, but chemical composition, maximum reached temperature, and heating/cooling histories are also contributing factors.

In this review we present studies on iron and stony meteorites as well as on tektites.

We report studies on two iron meteorites, one of them belonging to the shower find of Campo del Cielo, and the other from an unknown find; this latter unregistered meteorite was named by us as "Find 1". In the Campo del Cielo find, a region belonging to the province of Chaco and Santiago del Estero, Argentina, there are samples characterized as octahedrites and others as hexahedrites [20]. This heterogeneity in the shower find was first proposed by Villar [21], and is the reason of our study on that specific meteorite. The unregistered stony meteorite, which we named "NWA 1990 stony"(1990 being a tentative lowest possible find date), was collected in Northwest Africa in the 1990s in the form of many small (centimetric) pieces, but it is not yet classified. We previously analyzed NWA 1990 stony in [22].

In earlier studies, we presented results on tektites from different strewn fields [23,24]. In the present study we refer to more tektites, as well as to the use of other experimental analytical methods in their study.

2. Materials and Methods

2.1. Samples

The studied iron meteorites are shown in Figure 1. They presented a black and irregular shape with regmaglypts. Not much oxidation was visible in the case of the unknown meteorite, so accordingly to chemical weathering classification [25], a W0 or W1 grade could be assigned. Their masses were about 26 g and 42 g, and their lengths were about 3.8 cm and 5.5 cm long, for the unknown iron meteorite and for the Campo del Cielo meteorite, respectively.
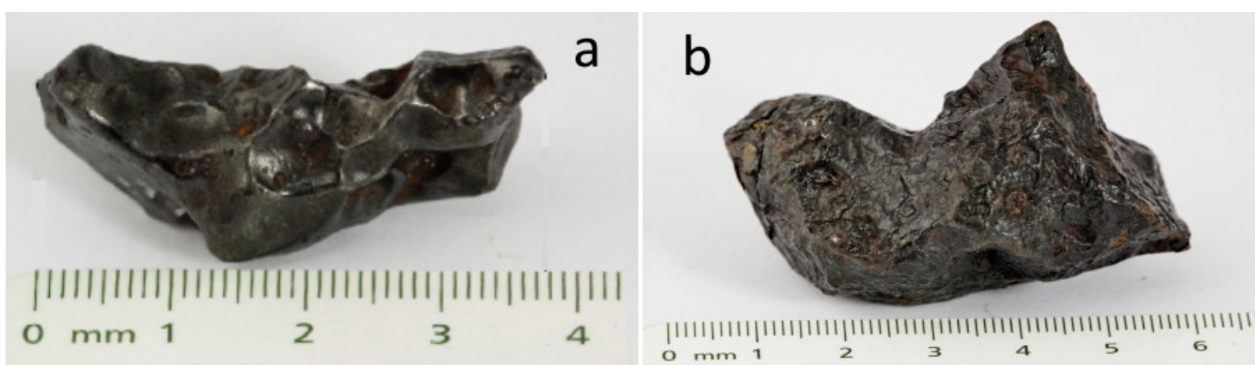
Figure 1. The studied iron meteorites: (**a**) Find 1 and (**b**) Campo del Cielo.

The NWA 1990 stony meteorite fragments have a dark crust but, after crushing, the powders reveal a brown-reddish color. Figure 2 shows typical images. After microscopic investigations, chondrules appear to be absent, so it was grouped in achondrites stony meteorites.
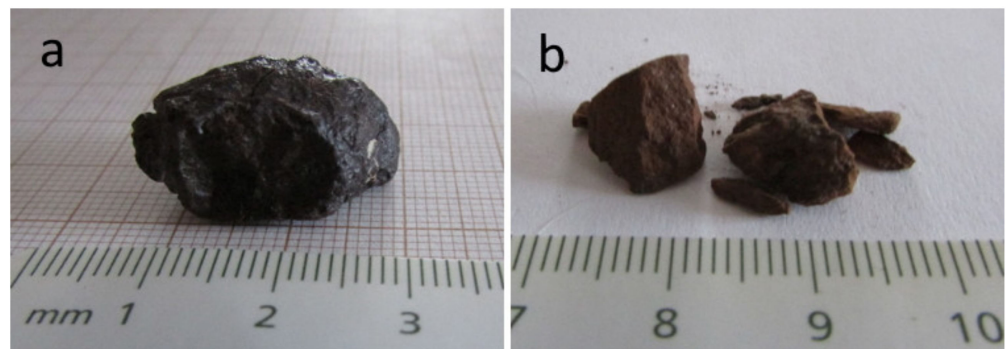
Figure 2. Typical NWA 1990 stony pieces: (**a**) a collected fragment, (**b**) crushed fragment.

Several tektites from different strewn fields were studied: moldavites, indochinites (including Muong Nong type), bediasites, chinites (including Guangdong tektites), rizalites, australites and other Australasian tektites from different locals. A Darwin glass from Tasmania was also studied. The indochinites studied were from Khon Kaen (10 samples) and Norm, Khorat Plateau (Thailand, 3 samples), the bediasites from Texas (4 samples), chinites from Leigong Mo (5 samples), rizalites from the Philippines (2 samples), an australite from Lake Yindalgooda, Australia, a moldavite from Chum Sud, Bohemia, and other Australasian samples from Laos, Vietnam, Tibet and Cambodia. Among the tektites studied there were three Muong Nong-type, two from Laos and one from China.

Figures 3–5 show examples of the samples.

Figure 3. Examples of studied tektites.

Figure 4. A Muong Nong tektite from Laos.

Figure 5. The studied Darwin glass sample from Tasmania.

Provenance of the samples:

- Campo del Cielo and Find 1 unregistered iron meteorites: acquired in a mineral show.
- NWA 1990 stony meteorite: kindly provided by Mr. Miguel Gonçalves, NEO Skytale, Castelo Branco, Portugal.
- Bediasites, rizalites, australite, and moldavite: kindly provided by Mr. Aubrey Whymark, Senior Wellsite Geologist and Geosteering Specialist, Qatar Petroleum.
- Thailandites: collected by one of us (EIA) in the field in NE Thailand, Khon Kaen district and Khorat Plateau.
- Muong Nong (Laos): acquired from Mr. Sivadol Rodrubboon, in NE Thailand, Khon Kaen district, near the Laotian border.
- Muong Nong (China): acquired from Mr. Gao Fu, in Hong Kong.
- Tibetanite: acquired from Mr. Mike Petrov, Canada, who claims he got it from the original collector.
- Vietnamite: acquired from Mr. Long Nguyen, Yen Bai, Vietnam.
- Cambodiaite: acquired from Mr. James Fowler, Siem Reap, Cambodia.
- The analyses performed on the samples were:
- Iron meteorites: optical, microprobe and scanning electron microscopies, X-ray diffraction and Mössbauer spectroscopy in the two geometries described in Section 2.4.
- Stony meteorite: optical, microprobe and scanning electron microscopies, X-ray diffraction and Mössbauer spectroscopy in transmission geometry.
- Tektites: optical microscopy, X-ray fluorescence, X-ray diffraction and Mössbauer spectroscopy in both the geometries described in Section 2.4.

2.2. Optical and Microprobe/Scanning Electron Microscopies

Optical microscopy was performed with reflected visible light using a Nikon Optiphot, Tokyo, Japan, and photos were taken varying the light source, position of the sample, and magnification. Microprobe analysis was performed in a JEOL JXA8200 microprobe, Tokyo, Japan, with an electron acceleration voltage of 15 kV. Scanning electron microscope was used to obtain images with different amplifications in a TESCAN VEGA3, Brno, Czech Republic with an electron acceleration voltage of 20 kV and using backscattered electrons and EDX detectors.

Prior to the observations the samples were cut into slices and polished.

2.3. X-ray Diffraction

X-ray diffraction (XRD) was performed at room temperature (RT) using a Bruker D8 Advance (Karlsruhe, Germany) powder diffractometer with Cu Kα radiation ($\lambda = 0.154184$ nm), in θ–2θ Bragg-Brentano geometry. The acquisition was usually in the 2θ range of 10–90° with a step of 0.03° and an acquisition time of 10 s per step. The diffractogram was empirically least-squares fitted using a reference data base.

2.4. X-ray Fluorescence

X-ray fluorescence (XRF) was used in two methods. One of them was done in pressed pellets (approx. 20 mg sample diluted in 2 g boronic acid) analyzed in a PANalytical aXios 4 kW instrument (Almelo, The Netherlands) applying standardless methods as implemented in the Super Q/OMNIAN V 5.0D program package (PANalytical B.V.). The second method was applied in a flat surface of the glasses using a Hitachi SEA6000VX (Tokyo, Japan) benchtop high-sensitivity analyzer equipped with a tungsten target. Four conditions were used in order to be able to detect the different elements. The X-ray tube operated at potentials of 15 and 50 kV, currents of 500 and 1000 mA and a 3 mm wide primary-beam collimator. The acquisition time was 180 s and different filters were used. The SEA6000 VX measurement geometry was fixed, with its energy-dispersive Vortex Si semiconductor detector positioned at a scattering angle of 135° and a distance of 19 mm from the specimen.

2.5. ^{57}Fe Mössbauer Spectroscopy

^{57}Fe Mössbauer spectra were recorded at RT in two ways: backscattering geometry using a MIMOS II spectrometer (Mainz, Germany) [26] (Figure 6) and transmission geometry using a WISSEL spectrometer (Stanberg, Germany). A ^{57}Co(Rh) source was used with an activity of about 80 mCi and 5 mCi, respectively. No sample preparation was needed in the case of backscattering geometry. The raw samples were measured, except the interior of meteorites, which were cut and then the cut face measured. Radiation penetration is about 400–500 μm, so that the surface of the samples, that oxidizes quickly, is the minor fraction to be probed. The surface volume/total volume ratio probed is about 2×10^{-4}% in our experimental conditions [23,24]. The problem still exists in non-flat surfaces. Natural surfaces, tektites, in particular, have plenty of holes that may contain soil materials, adding Fe^{3+} to MS spectra. The measured samples were cleaned to remove all materials not belonging to the studied items. In the case of iron meteorites an additional advantage of using backscattering geometry exists; the avoidance of solid-state transformation, namely of γ-phase to α-phase induced by filing the metal [27]. In the case of transmission geometry, the preparation method was different for each type of sample; pieces of iron meteorites were filed to powder (60 μm diameter) using a diamond file; the stony meteorite was simply crushed down; the tektites were crushed immersed in silicon oil in order to prevent oxidation.

Figure 6. MIMOS II spectrometer measuring an iron meteorite placed on top of the window.

The Miniaturized Mössbauer Spectrometer (MIMOS II) performs the non-destructive measuring of samples. Due to its miniaturization and backscattering geometry it is lightweight, portable, and therefore used in a wide range of Mössbauer applications, especially where no sample preparation is possible. It works over a wide temperature range ($-120\,°C$ to $+40\,°C$) and has low power consumption. It also measures simultaneously 14.4 keV gamma-rays and 6.4 keV Fe-X-rays. MIMOS II was designed for Mars expeditions but has been used in several terrestrial applications as well, e.g., industrial applications, environment and soil analysis, and archaeology studies.

All meteorites' spectra were analyzed using a set of Lorentzian lines determined by least squares method while, in the case of tektites, the fitting procedure of the obtained spectra was carried out using a set of Voigt lines and parameters determined by least squares. This method has already been proved to be adequate to adjust hyperfine parameters of glasses, in particular tektites [23,24,28,29]. The use of Voigt lines instead of Lorentzian lines in the case of tektites was chosen because of the high degree of their amorphization. The isomer shifts are given relative to α-Fe at RT.

3. Results

3.1. Iron Meteorites

Microstructure analysis on polished slices shows that a Widmanstätten pattern and schreibersite microcrystals (($Fe, Ni)_3P$) are evident in the Campo del Cielo fragment. The Find 1 iron meteorite does not exhibit Widmanstätten patterns but shows Neumann bands along with schreibersite microcrystals [30–32]. Microstructures of each meteorite are shown in Figure 7.
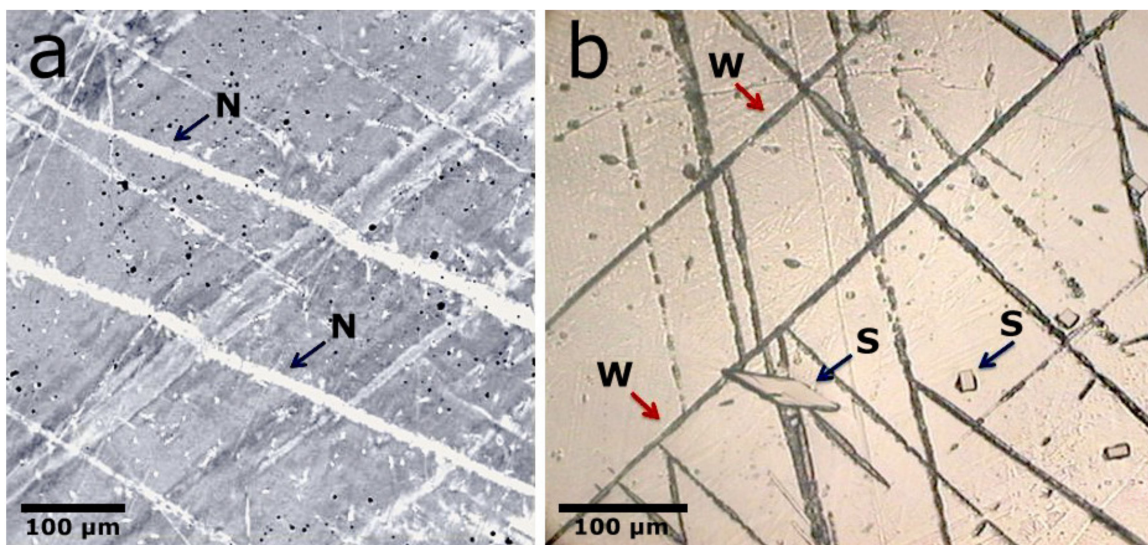
Figure 7. Micrographs of (**a**) unregistered iron meteorite showing Neumann bands (N), and (**b**) Campo del Cielo meteorite demonstrating Widmanstätten patterns (W) and Schreibersite crystals (S). (**a**) Electron microprobe micrograph and (**b**) optical micrograph.

Figures 8 and 9 show microprobe analysis images of polished sections of the iron meteorites' fragments. The inclusions observed have the shape of schreibersite microcrystals and the composition (Table 1), with high phosphorous content, is in agreement with the presence of this mineral. The matrix is composed mainly of iron with small content of nickel being consistent with kamacite. In Table 1 the elementary composition of the main elements is shown for each meteorite.
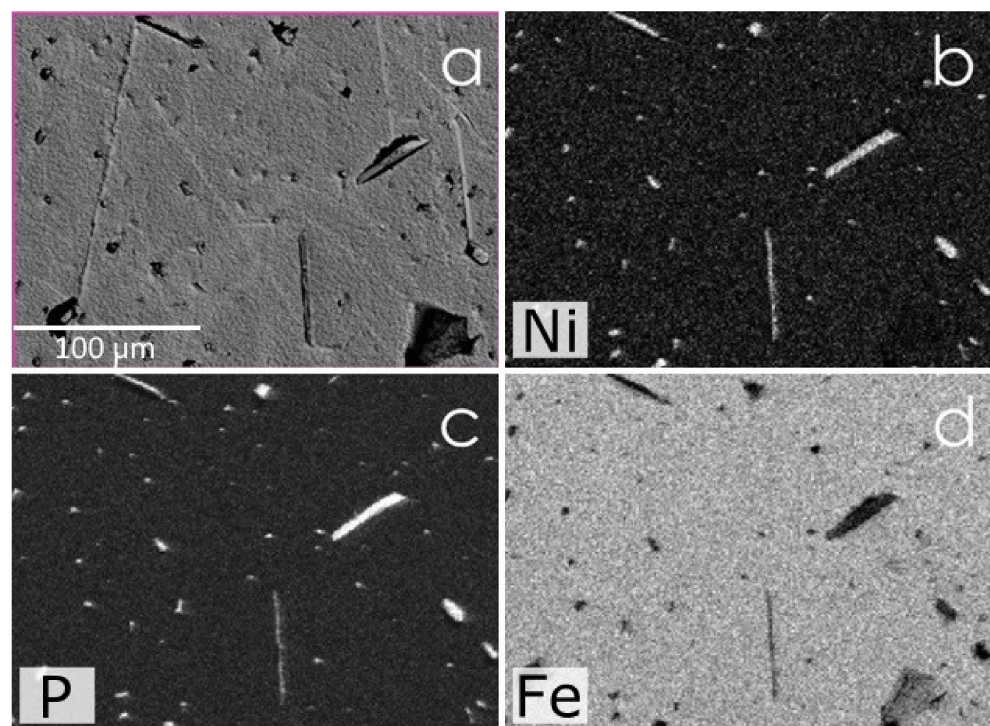
Figure 8. Micrograph (**a**) and elemental mapping obtained by microprobe analysis for Ni (**b**), P (**c**) and Fe (**d**) for the Find 1 iron meteorite [31].
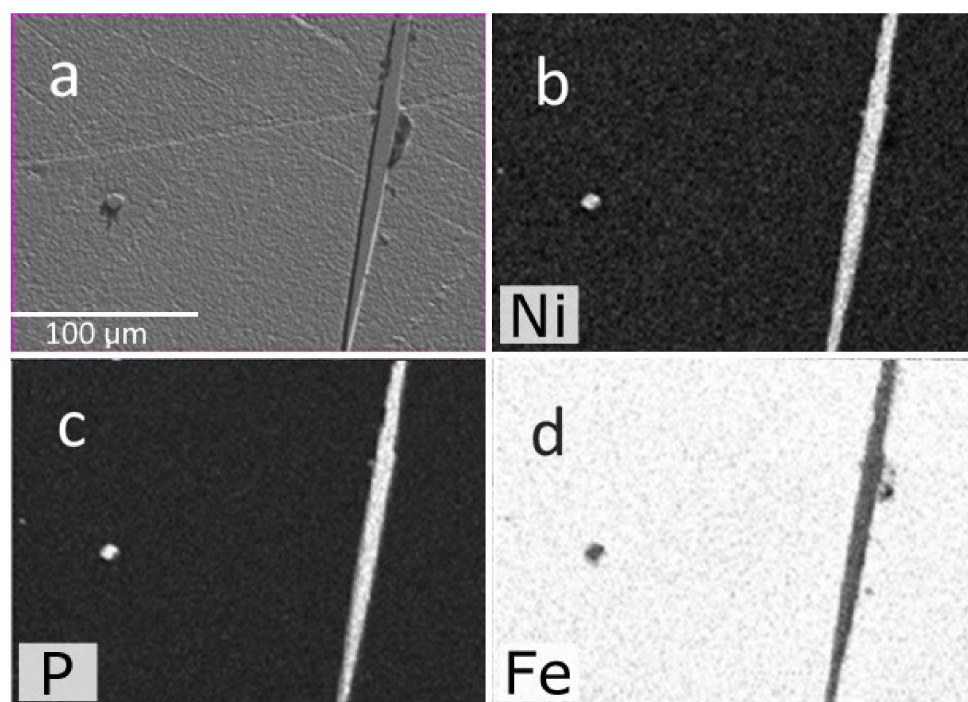
Figure 9. Micrograph (**a**) and elemental mapping obtained by microprobe analysis for Ni (**b**), P (**c**) and Fe (**d**) for the Campo del Cielo meteorite [31].

Table 1. Elemental composition of the meteorites determined by microprobe analysis [31].

Meteorite	Mineral	Fe (wt.%)	Ni (wt.%)	P (wt.%)	Other
Find 1	Kamacite (matrix)	93.4 ± 0.4	5.71 ± 0.02	0.090 ± 0.007	Na, K, Cr, Co
	Schreibersite	52.5 ± 0.8	34.6 ± 0.50	11.93 ± 0.08	Na, K, Al, Mg
Campo del Cielo	Kamacite (matrix)	95.4 ± 0.7	6.20 ± 0.02	0.062 ± 0.01	Na, Co, Al, Cr
	Schreibersite	50.8 ± 0.8	35.3 ± 0.04	12.42 ± 0.07	Mn, Al, Ti

Figure 10 shows EDX maps for the Find 1 iron meteorite, taken with a scanning electron microscope. A schreibersite inclusion is observed in a fissure starting from the border of the meteorite.

X-ray diffraction performed at room temperature evidences only kamacite (bcc α-Fe(Ni, Co)) in the interior of both meteorites, but the diffraction patterns of their crusts reveal maghemite and goethite as weathering oxides, in the case of the Find 1 iron meteorite and in the case of Campo del Cielo meteorite magnetite as well, of which the surface was cleaned from terrestrial weathering.

For X-ray diffraction of the interior of meteorites, the same slices used for microscopy were used while, for the crust, the powder resulting from filing the crust was used.

Mössbauer spectra confirms the existence of kamacite in the interior of meteorites, this being the only phase determined in the Find 1 iron meteorite (Figure 11). The hyperfine parameters are similar to those obtained for iron meteorites studied by dos Santos et al. [33], such as Toluca or Itutinga, which also consist only of kamacite. It is known [34] that different Fe(Ni, Co) phases in a meteorite can be found related to Ni content: α-Fe(Ni, Co) with Ni $\leq$ 7 wt.%, α_2-Fe(Ni, Co) with 15–25 wt.% of Ni and γ-Fe(Ni, Co) with 25–50 wt.% of Ni.
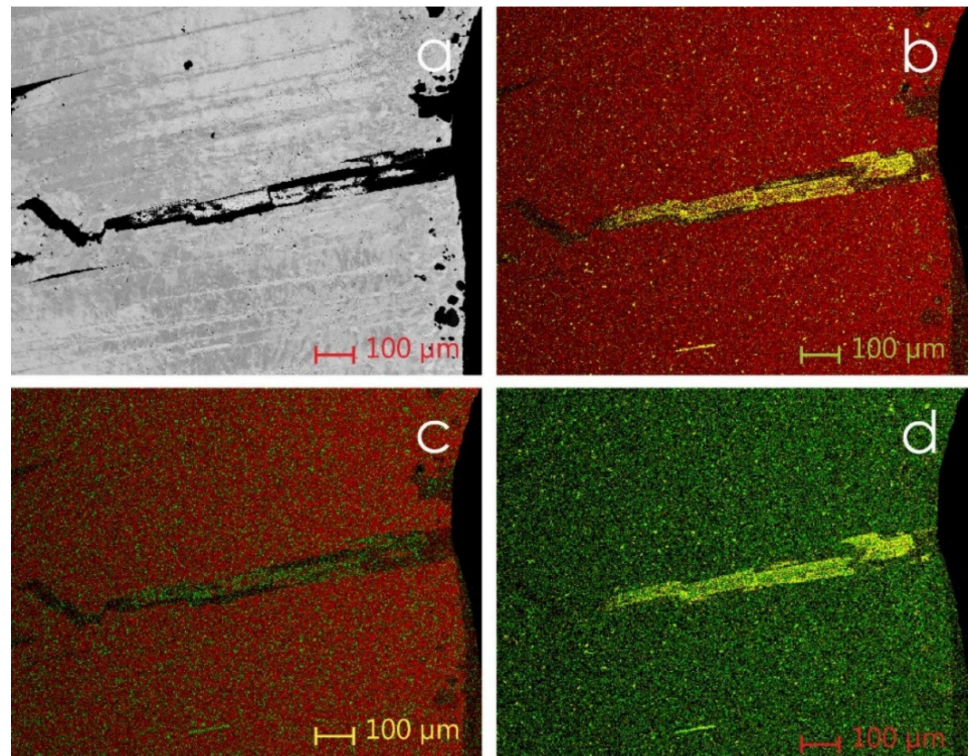
Figure 10. SEM micrograph (**a**) and associated X-ray maps (**b**–**d**) showing the distribution Fe, Ni and P in red, green and yellow respectively for Find 1 iron meteorite [30].
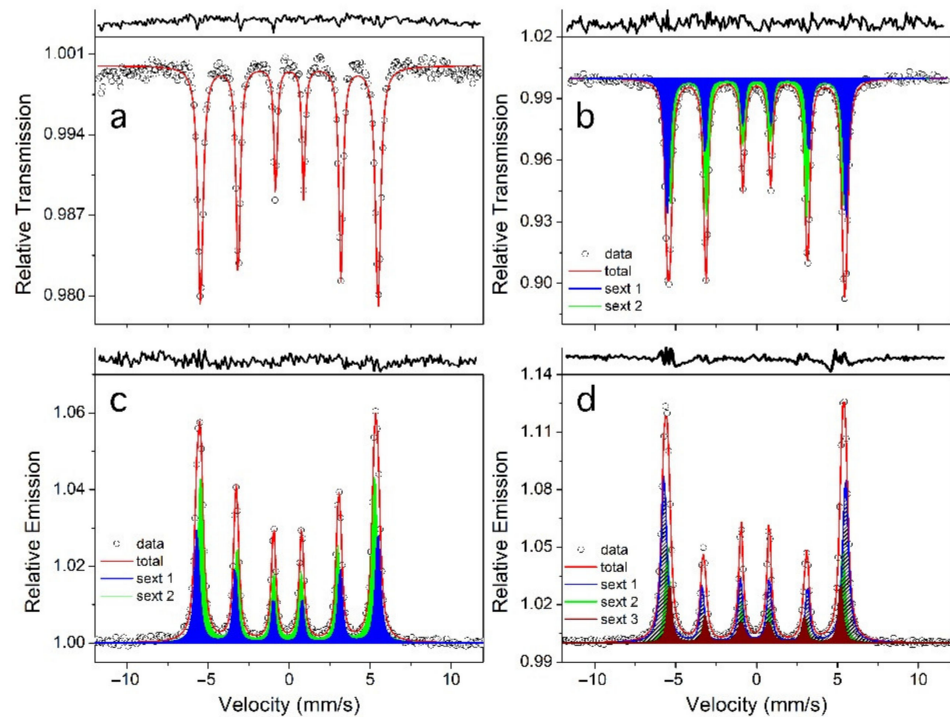
Figure 11. Mössbauer spectra of the interiors of Find 1 iron meteorite (**a**,**c**) and Campo del Cielo meteorite (**b**,**d**) measured at RT in transmission (**a**,**b**) and backscattering (**c**,**d**) geometries.

In backscattering geometry, the spectrum of the Find 1 iron meteorite was fitted with 2 sextets, Sext 1 being attributed to α_2-Fe(Ni, Co) and Sext 2 attributed to α-Fe(Ni, Co) [33,34]. The first phase is martensite in lamellae or plessite and the other is kamacite and richer in Ni. The abundance of the second phase is almost twice the abundance of the first phase (see Table 2).

Table 2. Mössbauer parameters obtained from the fitting to the spectra shown in Figure 11 [31]. The errors in the last digit are given in brackets.

Meteorite	Geometry	IS (mm/s)	2ε (mm/s)	B (T)	Γ (mm/s)	%	Subspectra
Find 1	Transmission	0.008(1)	−0.015(1)	34.0(1)	0.32(1)	100	Sext
	Backscattering	0.006(1)	−0.015(1)	34.7(1)	0.30(1)	37.5	Sext 1
		0.004(1)	0.009(1)	33.4(1)	0.32(1)	62.5	Sext 2
Campo del Cielo	Transmission	0.090(1)	−0.019(1)	34.3(1)	0.30(1)	43.3	Sext 1
		0.080(1)	0.020(1)	33.3(1)	0.32(1)	56.7	Sext 2
	Backscattering	0.010(1)	−0.016(1)	34.7(1)	0.30(1)	52.0	Sext 1
		0.012(1)	0.010(1)	33.4(1)	0.33(1)	35.8	Sext 2
		0.029(1)	0.014(1)	31.5(1)	0.60(1)	12.2	Sext 3

In the case of Campo del Cielo meteorite, already in transmission geometry the two phases are observed, while in backscattering geometry γ-Fe(Ni, Co) is also found (Sext 3) [34,35]. This result shows that filing the sample for the transmission measurement may have transformed the γ phase into α phase. To be sure of that, one should compare metal powders prepared under different conditions, like in the work of Oshtrakh et al. [34], work that is being prepared.

Taenite is present in several meteorites as also observed by dos Santos et al. [33]. On the other hand, tetrataenite (ordered taenite γ-FeNi) or paramagnetic γ-Fe(Ni, Co) phases were not observed in Campo del Cielo. As referred by Scorzelli et al. [36] and dos Santos et al. [33], to allow the formation of tetrataenite the meteorite should have been cooled down at a very slow cooling rate, at temperatures below 320 °C and subsequently not be subjected to a strong shock. The question of whether this meteorite cooled too fast or was shocked may eventually be answered by performing electron probe microanalyzer Ni-profiles within taenite crystals as suggested by Goldstein et al. (e.g., [25,37]). We have not done it for the present paper, but it remains a major priority for future work.

A fragment of Campo del Cielo fall, referred as a hexahedrite meteorite, was studied by Cabanillas et al. [20]. Their work shows Mössbauer spectra of the surface and interior of the meteorite, but no parameters from the fitting procedure are given. The spectrum of the internal region is similar to the spectrum of Campo del Cielo meteorite obtained by us, and the surface spectrum exhibits a magnetic contribution assigned to oxides and a quadrupole interaction.

Figure 12 shows the Mössbauer spectra of the crusts (both fusion and terrestrial weathering) of meteorites in transmission and backscattering geometries. Table 3 gives the hyperfine parameters determined in the fitting procedure. In this figure, besides kamacite, several weathering products can be observed.

In general, iron oxides as maghemite, lepidocrocite, akaganite, and goethite are often found as weathering products of iron meteorites [38].

For the Find 1 iron meteorite the same phases are found in both geometries; Sext 1 is attributed to maghemite, a weathering product, Sext 2 is attributed to kamacite and a Fe^{3+} doublet, from weathering. This doublet is a relatively large component of the spectra and has a magnitude of splitting that usually is not specific from the mineral, and can be a combination of several phases, as superparamagnetic hematite or goethite, lepidocrocite, akaganite, ferrihydrite and phyllosilicates [38]. As in XRD patterns we saw the presence of goethite, the Fe^{3+} doublet can be assigned to superparamagnetic goethite, meaning that this phase exists in very small particles.
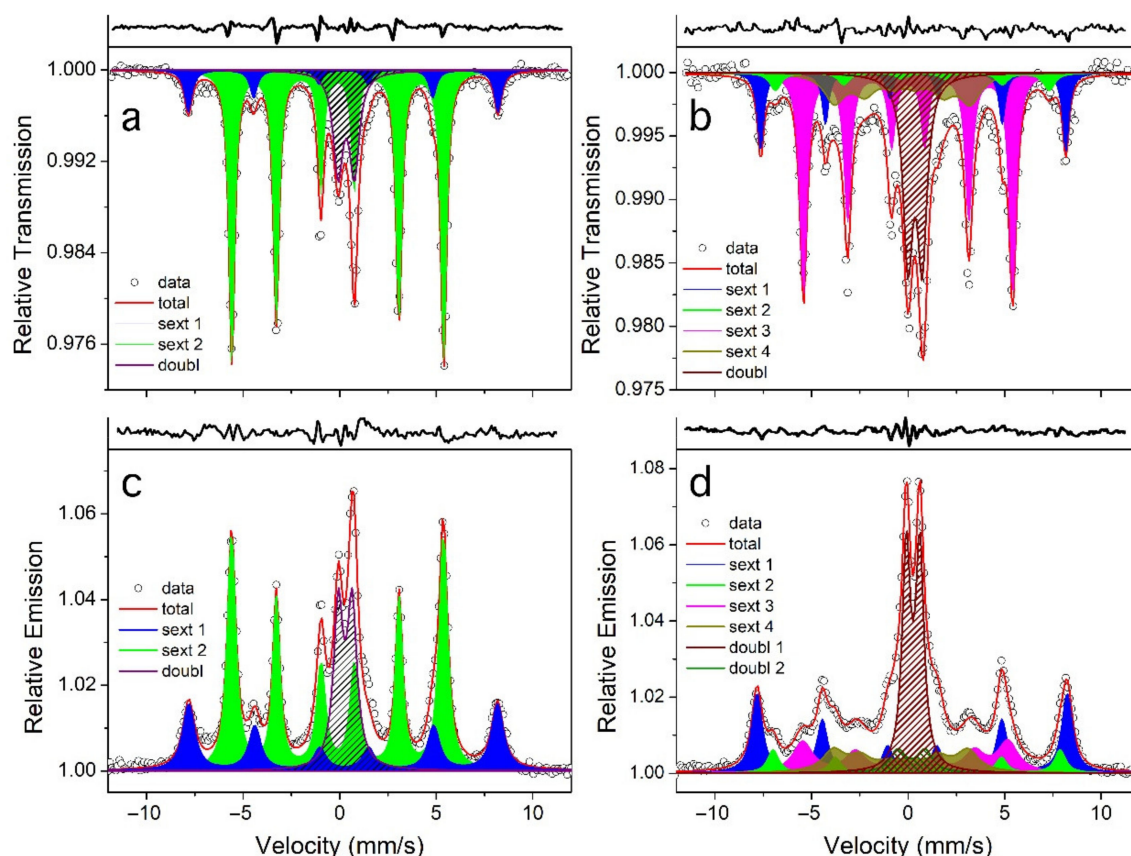
Figure 12. Mössbauer spectra of the exterior part of Find 1 iron meteorite (**a**,**c**) and Campo del Cielo meteorite (**b**,**d**) measured at RT in transmission (**a**,**b**) and backscattering (**c**,**d**) geometries.

Table 3. Mössbauer parameters obtained from the fitting to the spectra shown in Figure 12 [31]. The errors in the last digit are given in brackets.

	Geometry	IS (mm/s)	2ε/QS (mm/s)	B (T)	Γ (mm/s)	%	Subspectra
Find 1	Transmission	0.29 (1)	0.01 (1)	49.7 (1)	0.45 (1)	11.7	Sext 1
		0.01 (1)	0.014 (1)	34.0 (1)	0.35 (1)	70.7	Sext 2
		0.45 (1)	0.85 (1)	−	0.61 (1)	17.6	Doubl
	Backscattering	0.32 (1)	0.06 (1)	49.5 (1)	0.75 (1)	22.5	Sext 1
		0.01 (1)	−0.01 (1)	34.0 (1)	0.50 (1)	56.5	Sext 2
		0.40 (1)	0.72 (1)	−	0.59 (1)	21.0	Doubl
Campo del Cielo	Transmission	0.39 (1)	0.03 (1)	49.0 (1)	0.41 (1)	13.6	Sext 1
		0.40 (1)	−0.10 (1)	45.6 (1)	0.70 (1)	5.2	Sext 2
		0.03 (1)	−0.005 (1)	33.6 (1)	0.45 (1)	42.5	Sext 3
		−0.14 (1)	−0.09 (1)	21.8 (1)	1.29 (1)	15.7	Sext 4
		0.47 (1)	0.74 (1)	−	0.60 (1)	23.0	Doubl
	Backscattering	0.32 (1)	−0.002 (1)	49.8 (1)	0.67 (1)	26.2	Sext 1
		0.60 (1)	−0.09 (1)	46.0 (1)	0.68 (1)	7.8	Sext 2
		0.02 (1)	−0.05 (1)	32.9 (1)	0.90 (1)	18.5	Sext 3
		−0.32 (1)	0.08 (1)	21.5 (1)	1.37 (1)	14.6	Sext 4
		0.31 (1)	0.70 (1)	−	0.50 (1)	27.5	Doubl 1
		0.27 (1)	1.44 (1)	−	0.95 (1)	5.4	Doubl 2

One can see that the kamacite component found in transmission geometry has a larger fraction than the one found in backscattering geometry, possibly a result of the filing procedure to obtain powder samples for the transmission measurement. The backscattering spectrum has larger linewidths showing a much higher degree of disorder of the phases.

The comparison of the fitting of the two spectra is not so immediate, as there are different absorption effects and the fitting quality is not the same. One can see a base line distortion, due to the cosine effect, in the case of the transmission spectrum.

In the case of Campo del Cielo meteorite, Sext 1 and Sext 2 are attributed to the two sites of magnetite, while Sext 3 belongs to kamacite and Sext 4 to a relaxation phase at RT. The doublet (Doubl 1) can also be goethite in very small particles. A second Fe^{3+} doublet (Doubl 2) is seen in the case of backscattering geometry. This doublet should be another superparamagnetic oxide-hydroxide.

It is evident that the weathering of Campo del Cielo fragment is much higher than that of the other iron meteorite, as the spectral components of oxides have larger contributions. Comparing the backscatter spectra of both raw meteorites one can see that there are weathering products also observed in Mars soil and meteorites (Meridiani Planum) specially the doublet assigned to nano-oxide nanoparticles [38].

We have observed the border of the meteorites by SEM (see Figure 13 for an example). SEM/EDX analysis confirmed the existence of oxides by the great amount of oxygen present. The need to use SEM/EBSD seems to be essential in a future work to determine the minerals present in them.
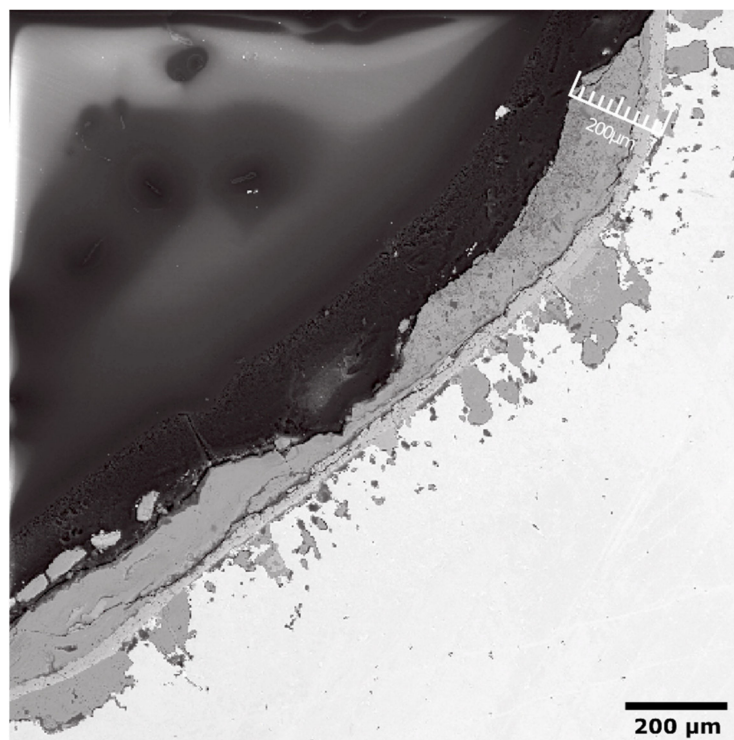

Figure 13. SEM micrograph obtained for Find 1 where the crust can be observed.

The results obtained so far, and shown here, indicate that the iron meteorite from the Campo del Cielo fall is an octahedrite and that the Find 1 iron is a hexahedrite. Of course, the general classification we offer for this unregistered meteorite shall be further refined in the future, namely when we perform Ge, Ga and Ir analyses [39].

3.2. Stony Meteorite

Microscope observations indicate that NWA 1990 stony is an achondrite.

Figure 14 shows a typical optical micrograph of the meteorite. One can observe a multi-mineral brecciated texture.
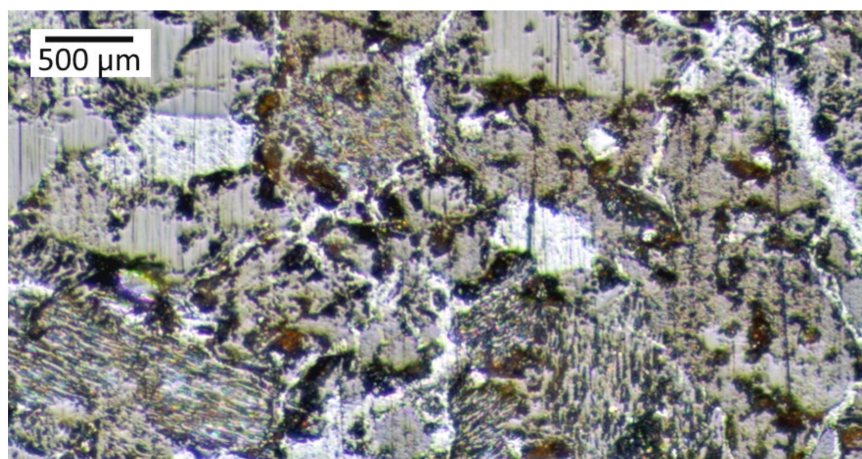
Figure 14. Typical optical micrograph of NWA 1990 stony meteorite.

The chemical composition of the meteorite is common for stony meteorites, with a large fraction of Si. The composition analysis, done by XRF with the second method described in Section 2.3, is shown in Table 4.

Table 4. Mean elemental composition of NWA 1990 stony meteorite excluding oxygen. The error in the values is 2%.

Element	Mean Concentration (wt. %)
Fe	39.4
Si	30.1
Mg	21.2
Al	3.5
Ni	1.9
Co	1.2
Ca	1.2
Cr	0.4
Na	0.4
P	0.3
Ti	0.3
K	0.1
Mn	0.1

We can see in Figure 15 that the elements are not uniformly distributed and, as expected, several phases with different compositions exist. Mössbauer spectroscopy (Figure 16) shows that the main element, Fe (39%), is only related to the abundance of maghemite and troilite. The RT spectrum is similar to that obtained for schreibersite pieces of Sikhote-Alin iron meteorite [40–43] but, in fact, in our case it shows superparamagnetic behavior with iron in trivalent coordination, as indicated in Table 5, and splits at 4.2 K. Most of the 4.2 K spectrum was fitted with the two sextets of maghemite expected at this temperature (see for instance [44]), plus a very small amount (1.1%) of troilite (FeS). Troilite was fitted with only one sextet, as explained in other works [45], instead of an octet. Other Fe-bearing phases, like kamacite, can be present and masked in the maghemite envelope, but most probably Fe-containing minerals within this meteorite are affected by weathering, which is observed to be very strong. This kind of weathering is common in chondrites found in hot deserts [46,47].
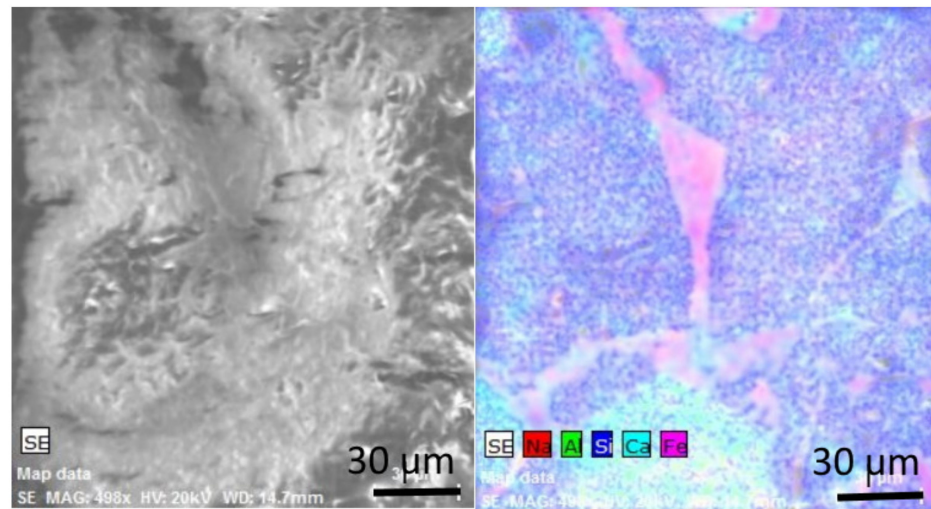
Figure 15. Backscattered electron image and associated EDX map obtained for some indicated elements.
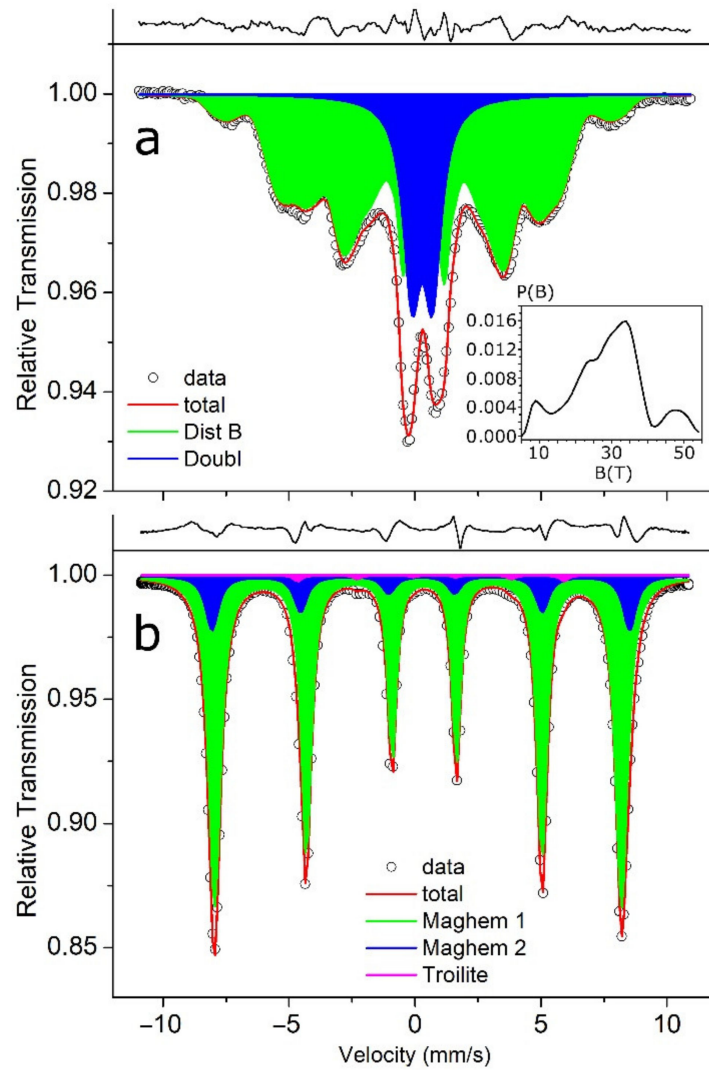

Figure 16. Mössbauer spectra obtained for NWA1990 stony meteorite at (**a**) RT and (**b**) 4.2 K. The inset in (**a**) represents the distribution of the hyperfine field.

Table 5. Mössbauer parameters obtained from the fitting to the spectra shown in Figure 16. The errors in the last digit are given in brackets.

Temp.	IS (mm/s)	2ε/QS (mm/s)	B (T)	Γ (mm/s)	%	Subspectra
RT	<0.35>	0	<29.1>	0.33 (1)	76.5	Dist B
	0.40 (1)	0.82 (1)		0.85 (1)	23.5	Doubl
4.2 K	0.48 (1)	−0.24 (1)	50.1 (1)	0.43 (1)	84.2	Magh 1
	0.48 (1)	−0.03 (1)	51.4 (1)	0.54 (1)	14.7	Magh 2
	0.93 (1)	−0.14 (1)	32.8 (1)	0.40 (1)	1.1	Troilite

The presence of troilite, together with a fusion crust, is evidence that this may indeed be a meteorite. Troilite can also be found, rarely, in Earth ultramafic rocks but, as far as we know, has never been reference in Northwest African ultramafics, namely in the Anti-Atlas belt. This result revealed by Mössbauer spectroscopy shows that this method may be useful in distinguishing between real and false meteorites, as referred by Bogusz et al. [48].

The XRD pattern (Figure 17) shows a lot of other silicate minerals. As we can deduct from Mössbauer spectrum at 4.2 K, iron is not included in those silicates. Actually, are only formed with other elements listed in Table 4. For instance, olivine is purely magnesian (forsterite—Mg_2SiO_4), orthopyroxene is also purely magnesian /enstatite-$MgSiO_3$). It is worth mentioning that for low angles there is a difference between experimental and calculated patterns, so that at least one additional phase is present. A mineral from the group of osumilite was found. Such a mineral has already been found in aubrites [49]. To confirm its occurrence in NWA 1990, SEM-EBSD measurements are envisaged for a future work.
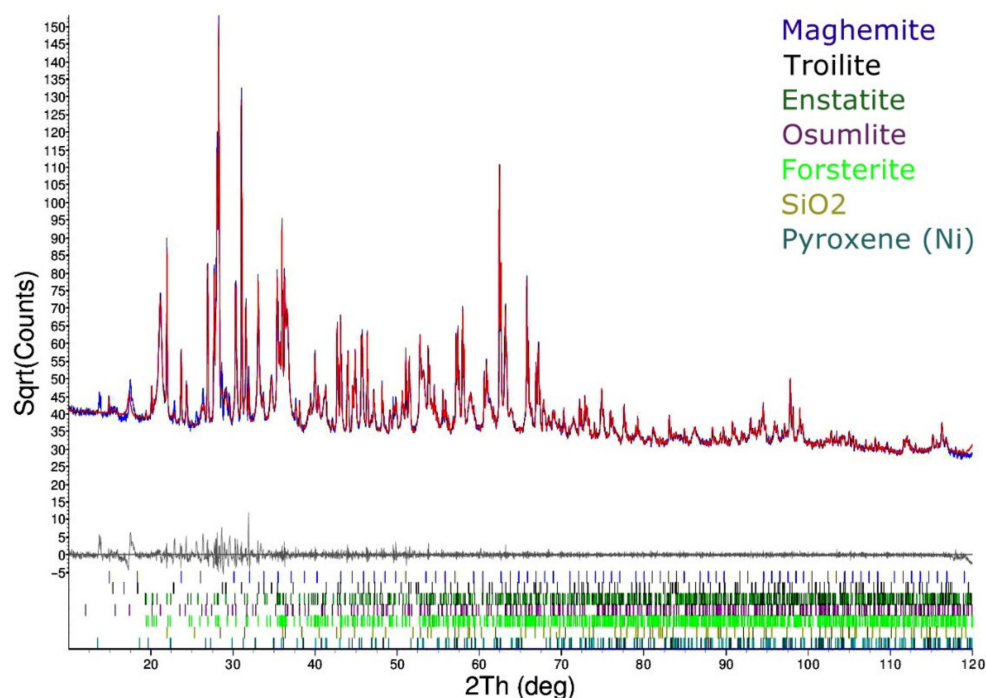

Figure 17. XRD pattern obtained at RT for the NWA 1990 stony meteorite and indexed phases.

The mineral assemblage found in our unregistered stony meteorite indicates that it is probably an enstatite achondrite (aubrite) [50,51]. Dunlap studied an enstatite chondrite from Abee, Canada, using Mössbauer spectroscopy [52] and also found troilite. In that study, other magnetic components at RT were found to be kamacite and taenite. Two paramagnetic phases were observed, niningerite and γ-FeNi. Maliszewski et al. [53] studied an enstatite achondrite from Zaklodzie, Poland, by Mössbauer spectroscopy. Troilite was also found, as well as kamacite, γ-FeNi and niningerite, for instance.
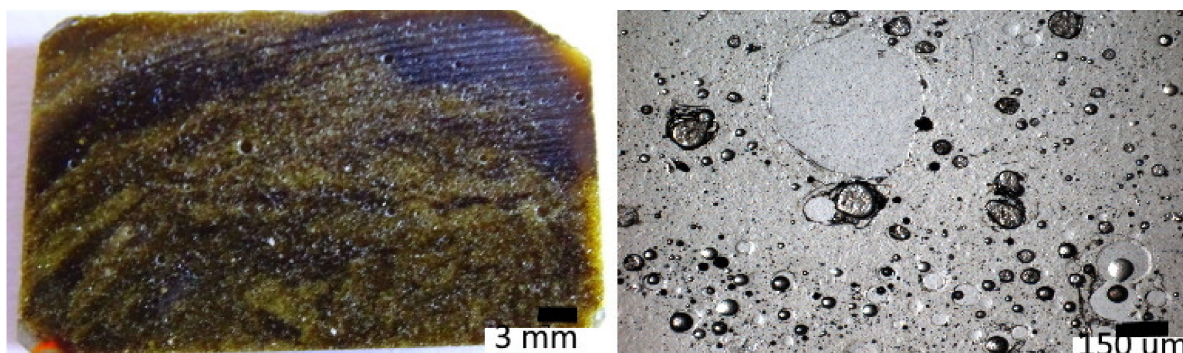
3.3. Tektites

In Figures 18 and 19, typical micrographs of polished sections of the studied glasses are observed.
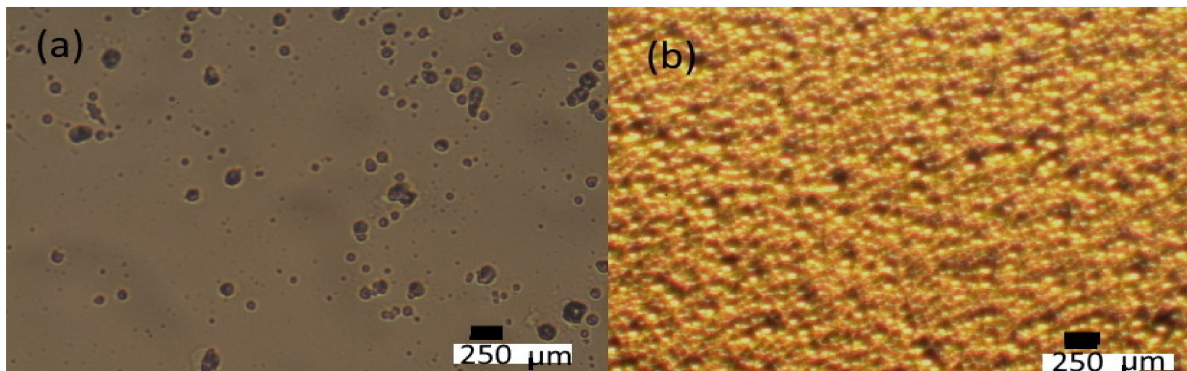
Figure 18. Optical micrographs of (**a**) a chinite and (**b**) Darwin glass.

Figure 19. A macrograph and an optical micrograph of a section of Muong Nong tektite from Laos (Laos-1 sample).

The micrograph of a chinite (Figure 18a) is typical of all other splash-form and aerodynamic tektites. There are no inclusions observed but some marks left by bubbles formed during melting and solidification of the glasses. X-ray diffraction carried out in such samples shows that they are amorphous. The Darwin glass (Figure 18b) is also amorphous and in the micrographs one can see a lot of bubble marks which cannot be observed with naked eye.

Figure 19 shows the layered structure of the Muong Nong, observed at naked eye (photograph on the left) and the micrograph calls the attention to inclusions as well as marks of bubbles. X-ray diffraction demonstrated that the sample is amorphous.

The composition of the studied tektites and the Darwin glass from Tasmania are shown in Tables 6 and 7. Two methods were applied for composition determination. The method used for the compositions shown in Table 7 indicates individual elements and it was not possible to quantitatively identify Na and Mg. This way, the values listed in both Tables cannot be directly compared.

One can verify that the compositions obtained for tektites are in general in accordance with the literature [6,7]. Ordinary tektites have typically about 70 wt.% of silica. Bediasites, for instance, have very low Mg and Ca, while moldavites are rich in Si and K, as observed in our case. The composition of the Darwin glass and the layered tektites (Muong Nong) are also in accordance with the literature [6–8].

Table 6. Average major elements chemical composition (oxide wt.%) of tektites from different strewn fields and the obsidian from Arizona, determined from XRF by the first method using PANalytical instrument. The error in the values is 2%.

	SiO$_2$	Al$_2$O$_3$	Na$_2$O	Fe$_2$O$_3$	MgO	CaCO$_3$	K$_2$O	TiO$_2$
Muong Nong (Laos)	70.12	18.45	2.79	2.52	2.94	1.42	1.25	0.40
Thailandite	70.53	17.17	3.02	2.74	2.90	1.62	1.62	0.31
Rizalite	71.09	15.67	2.74	2.34	2.34	3.63	1.55	0.32
Chinite	70.94	15.61	2.81	3.32	2.51	2.34	1.56	0.79
Australite	72.20	13.40	1.57	2.81	3.07	3.95	1.84	0.80
Bediasite	73.54	17.46	3.35	2.58	1.13	0.63	0.91	0.20
Moldavite	80.10	9.56	0.52	1.23	2.21	1.60	2.95	0.31
Darwin Glass	82.16	8.46	0.04	3.58	0.69	0.03	2.13	0.61

Table 7. Average major elements chemical composition (wt.%) of Australasian tektites determined from XRF by the second method using SEA6000 instrument. The method does not allow the determination of Na and Mg contents. The error in the values is 2%.

	Si	Al	Fe	Ca	K	Ti
Muong Nong (Laos-2)	77.62	12.01	2.54	2.43	2.31	0.52
Muong Nong (China)	76.81	12.02	3.02	3.80	2.43	0.61
Tibet	70.21	9.24	1.65	1.35	1.42	0.35
Vietnam	73.42	9.61	1.84	1.83	1.54	0.32
Cambodia	78.12	11.31	3.15	2.35	2.25	0.51

Mössbauer spectroscopy was performed at room temperature in all the samples, some in backscattering geometry and others in transmission geometry. We have used Voigt functions and discrete spectral components determined by the least squares fits. In general, the results of Mössbauer spectroscopy for the Fe-oxidation state ratios in tektites depends on the method of analysis. The analysis using discrete spectral components with Lorentzian functions give in general, anomalous results [54]. We have obtained consistent and homogeneous parameters within the same strewn field. For the tektites of the same strewn field averages of parameters were considered after fitting and are shown in Tables 6 and 7. Typical spectra are shown in Figures 20 and 21. The Mössbauer spectra have a similar shape with an apparently single asymmetric doublet, a characteristic shape of glass that contains mainly ferrous iron. The absence of sextuplets is due to the diluted nature of the glasses and indicates the absence of magnetic phases, also for the Darwin Glass. On the contrary, several Mössbauer studies on impactites show the presence of magnetic phases on those systems, e.g., [55–57]. The widening effects of the peaks are important in the glass spectra where the line widths are in the order of 0.60 mm/s. The Mössbauer spectra were used to estimate the fraction of each iron species, assuming that the peak area is directly proportional to the amount of iron in each site. We obtained hyperfine values for Fe^{2+} in both octahedral and tetrahedral coordination, as well as for Fe^{3+} ion coordination. The doublet corresponding to ferrous iron in tetrahedral coordination is not always seen in the spectra of tektites, when fitted with a distribution of parameters [58]. However, some authors have already fitted the corresponding spectra including these iron species [10,54,59].

As one can observe, the area of Fe^{3+} and Fe^{2+} in tetrahedral coordination is very small, so a unique fit is not an accomplished task. However, for each spectrum we chose the configuration fit with the lowest goodness parameter. It is worth mentioning that the spectra taken in transmission geometry are in good agreement with the ones taken in backscattering geometry.
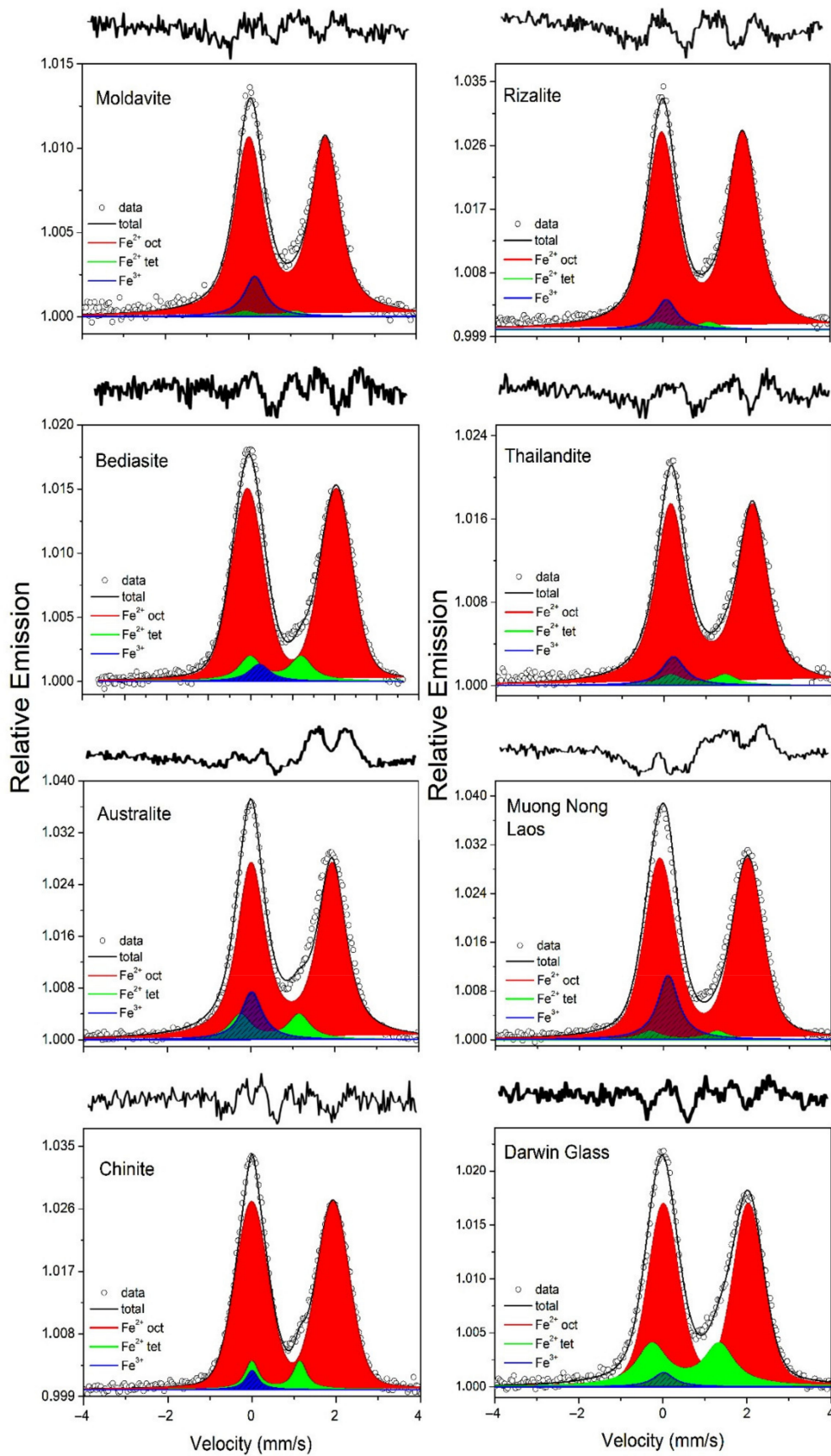
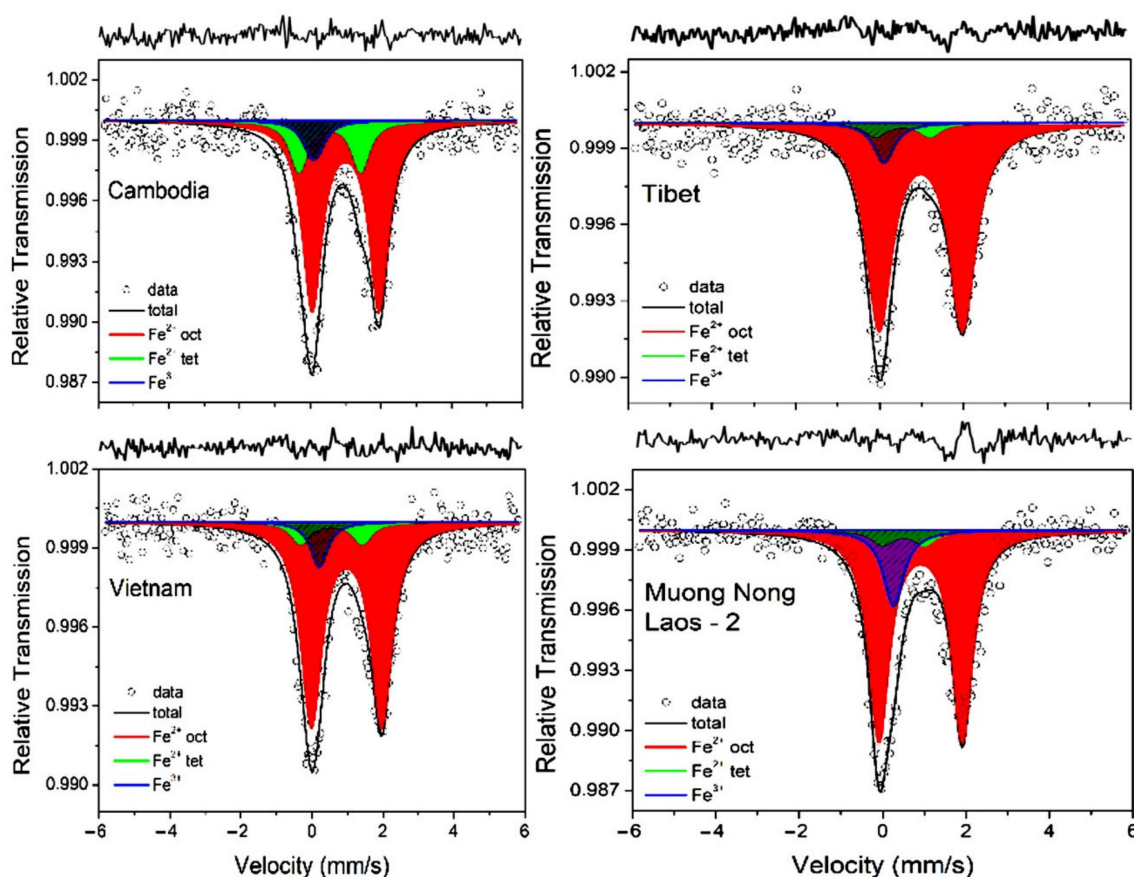**Figure 20.** Representative ^{57}Fe Mössbauer spectra taken at RT in backscattering geometry of typical tektites.

Figure 21. ^{57}Fe Mössbauer spectra taken at RT in transmission geometry of some groups of tektites.

The variations in the Fe^{3+}/Fe^{2+} ratio during the solidification of the molten material correspond to the absorption of oxygen on the sample surface from its environment. As seen in Tables 6 and 7, the mean Fe^{2+} octahedral isomer shifts values are within the range reported in the literature, typically +0.92 to +1.02 mm/s, and the mean quadrupole splitting values lie among the ones reported in the literature (typically 1.94 mm/s). Dunlap et al. [10,54,59] have used Voigt based analysis to determine isomer shift and quadrupole splitting distributions. Those authors have similar average isomer shifts for Fe^{2+} in octahedral coordination but much smaller values for quadrupole splitting. The Fe^{3+}/Fe^{2+} ratio observed in tektites is abnormally low compared, for example to terrestrial volcanic rocks, suggesting that they solidified in an environment with little oxygen, such as high temperatures and reduced conditions. Muong Nong tektites are examples of relatively high Fe^{3+}/Fe^{2+} ratio. These ratios are also shown in Tables 8 and 9, for tektites measured in backscattering geometry and transmission geometry, respectively. Those values are higher than those obtained by Dunlap et al. [10,54,59], but consistent within each strewn field. Additionally, for the Muong Nong tektites we have obtained higher Fe^{3+}/Fe^{2+} ratios than for other tektites. Impactites, including Darwin Glasses, have lower contents of Fe^{2+} octahedral component than tektites [60]. We have accordingly obtained 75% of Fe^{2+} in octahedral coordination against 80–90% in tektites, but with similar hyperfine parameters. To verify the ratios of Fe coordination, one can use a complementary technique, such as EXAFS, which we will try to use in a future work.
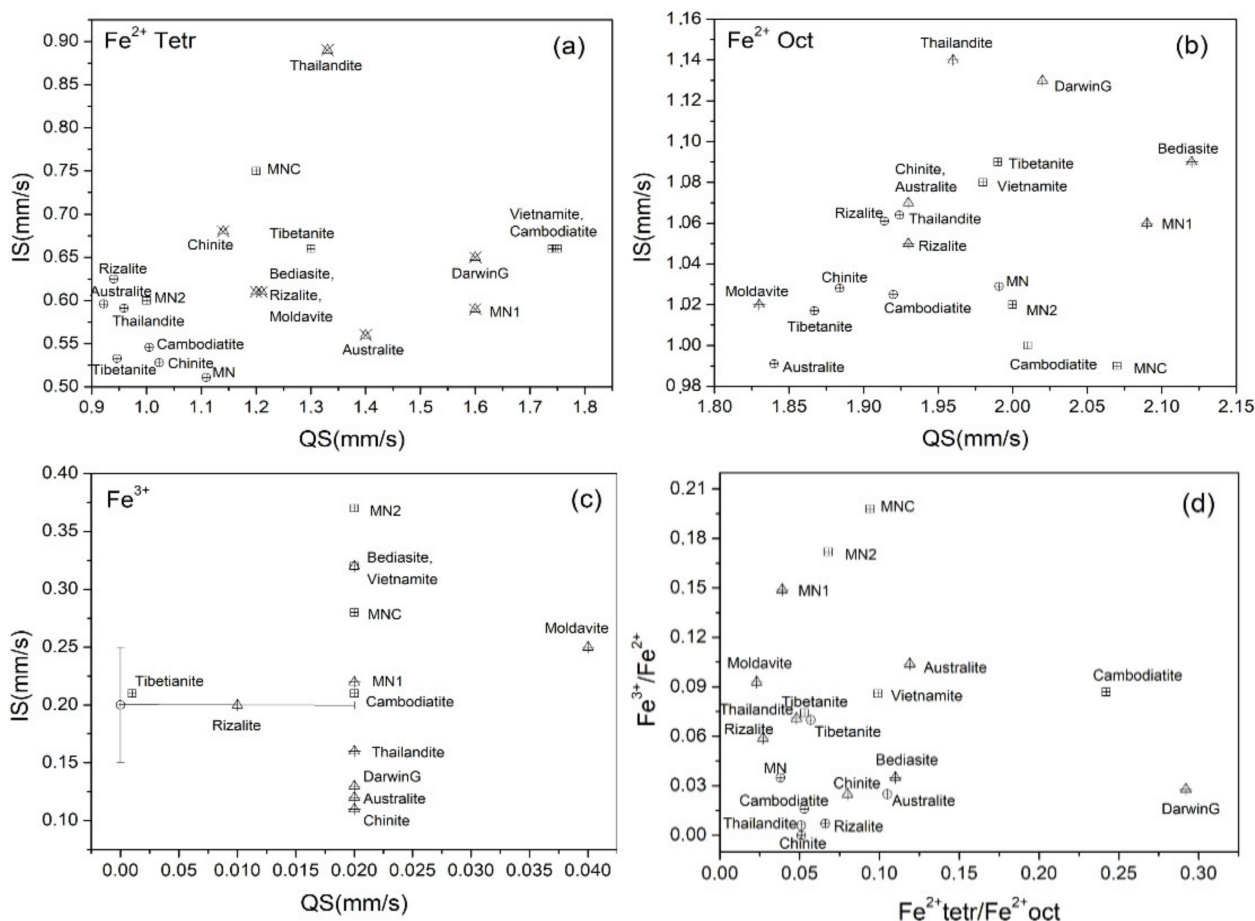
Table 8. Average hyperfine parameters obtained from the fitting procedure to spectra shown in Figure 20 for the different strewn fields. Errors in last significant digits are given in brackets.

Tektite	IS (mm/s)	QS (mm/s)	WID (mm/s)	%	χ^2	Fe^{2+}tetr/Fe^{2+}oct	Fe^{3+}/Fe^{2+}
Muong Nong (Laos)—MN1					1.90	0.038 (7)	0.149 (7)
Fe^{2+} Oct	1.06 (1)	2.09 (1)	0.60 (1)	83.8 (6)			
Fe^{2+} Tetr	0.59 (1)	1.60 (1)	0.60 (1)	3.2 (6)			
Fe^{3+}	0.22 (1)	0.02 (1)	0.60 (1)	13.0 (6)			
Thailandite					1.80	0.048 (7)	0.071 (6)
Fe^{2+} Oct	1.14 (1)	1.96 (1)	0.65 (1)	89.0 (6)			
Fe^{2+} Tetr	0.89 (1)	1.33 (1)	0.65 (1)	4.3 (6)			
Fe^{3+}	0.16 (1)	0.02 (1)	0.65 (1)	6.7 (6)			
Rizalite					1.92	0.027 (7)	0.059 (6)
Fe^{2+} Oct	1.05 (1)	1.93 (1)	0.60 (1)	91.9 (6)			
Fe^{2+} Tetr	0.61 (1)	1.20 (1)	0.60 (1)	2.5 (6)			
Fe^{3+}	0.20 (1)	0.01 (1)	0.60 (1)	5.6 (6)			
Chinite					1.63	0.080 (7)	0.025 (6)
Fe^{2+} Oct	1.07 (1)	1.93 (1)	0.60 (1)	90.4 (6)			
Fe^{2+} Tetr	0.68 (1)	1.14 (1)	0.50 (1)	7.2 (6)			
Fe^{3+}	0.11 (1)	0.02 (1)	0.50 (1)	2.4 (6)			
Australite					1.81	0.119 (8)	0.104 (7)
Fe^{2+} Oct	1.07 (1)	1.93 (1)	0.60 (1)	81.0 (6)			
Fe^{2+} Tetr	0.56 (1)	1.40 (1)	0.60 (1)	9.6 (6)			
Fe^{3+}	0.12 (1)	0.02 (1)	0.60 (1)	9.4 (6)			
Bediasite					1.73	0.110 (7)	0.035 (6)
Fe^{2+} Oct	1.09 (1)	2.12 (1)	0.60 (1)	87.0 (6)			
Fe^{2+} Tetr	0.61 (1)	1.21 (1)	0.60 (1)	9.6 (6)			
Fe^{3+}	0.32 (1)	0.02 (1)	0.60 (1)	3.4 (6)			
Moldavite					1.40	0.022 (7)	0.093 (7)
Fe^{2+} Oct	1.02 (1)	1.83 (1)	0.60 (1)	89.5 (6)			
Fe^{2+} Tetr	0.61 (1)	1.20 (1)	0.60 (1)	2.0 (6)			
Fe^{3+}	0.25 (1)	0.04 (1)	0.60 (1)	8.5 (6)			
Darwin Glass					1.61		
Fe^{2+} Oct	1.13 (1)	2.02 (19	0.60 (1)	75.3 (6)		0.292 (8)	0.028 (6)
Fe^{2+} Tetr	0.65 (1)	1.60 (1)	0.85 (2)	22.0 (6)			
Fe^{3+}	0.13 (1)	0.02 (1)	0.60 (1)	2.7 (6)			

Table 9. Average hyperfine parameters obtained from the fitting procedure to spectra shown in Figure 21 for some groups of tektites. Errors in last significant digits are given in brackets.

	IS (mm/s)	QS (mm/s)	WID (mm/s)	%	χ^2	Fe^{2+}tetr/Fe^{2+}oct	Fe^{3+}/Fe^{2+}
Vietnam					1.13	0.099 (7)	0.086 (7)
Fe^{2+} Oct	1.08 (1)	1.98 (1)	0.72 (1)	83.8 (6)			
Fe^{2+} Tetr	0.66 (1)	1.74 (1)	0.65 (1)	8.3 (6)			
Fe^{3+}	0.32 (1)	0.02 (1)	0.60 (1)	7.9 (6)			
Tibet					1.41	0.053 (7)	0.074 (6)
Fe^{2+} Oct	1.09 (1)	1.99 (1)	0.76 (1)	88.4 (6)			
Fe^{2+} Tetr	0.66 (1)	1.30 (1)	0.60 (1)	4.7 (6)			
Fe^{3+}	0.21 (1)	0.001 (1)	0.60 (1)	6.9 (6)			
Cambodia					1.14	0.242 (8)	0.087 (7)
Fe^{2+} Oct	1.00 (1)	2.01 (1)	0.67 (1)	74.0 (6)			
Fe^{2+} Tetr	0.66 (1)	1.75 (1)	0.60 (1)	18.0 (6)			
Fe^{3+}	0.21 (1)	0.02 (1)	0.60 (1)	8.0 (6)			
Muong Nong (Laos-2)					1.55	0.068 (8)	0.172 (7)
Fe^{2+} Oct	1.02 (1)	2.00 (1)	0.60 (1)	79.9 (6)			
Fe^{2+} Tetr	0.60 (1)	1.00 (1)	0.60 (1)	5.4 (6)			
Fe^{3+}	0.37 (1)	0.02 (1)	060 (1)	14.7 (6)			
Muong Nong (China)					1.73	0.094 (8)	0.198 (8)
Fe^{2+} Oct	0.99 (1)	2.07 (1)	0.80 (1)	76.3 (6)			
Fe^{2+} Tetr	0.75 (1)	1.20 (1)	0.70 (1)	7.2 (6)			
Fe^{3+}	0.28 (1)	0.02 (1)	0.65 (1)	16.5 (6)			

Based on data in Tables 8 and 9, we plotted relevant charts for the available hyperfine parameters (Figure 22). In the plots there is also data reported on Dunlap et al. [54] for several strewn fields' tektites. For the adjustment of spectra, Dunlap et al. used fixed isomer shift and quadrupole splitting for the Fe^{3+} site, which is represented, together with the fixed interval, in Figure 22c.

Figure 22. Average hyperfine parameters of analyzed tektites plotted with data from Table 8 (triangles) and Table 9 (squares) and Dunlap et al. [54] (circles). (**a**) Fe^{2+}tetr; (**b**) Fe^{2+}oct; (**c**) Fe^{3+}; (**d**) (Fe^{3+}/ Fe^{2+}) vs (Fe^{2+}tetr/ Fe^{2+}oct). MN1: Laos Muong-Nong 1; MN2: Laos Muong-Nong 2; MNC: Chinese Muong-Nong.

Comparing our results with the ones obtained by Dunlap et al. [54] we can see that for Fe^{2+} octahedral site, the hyperfine values are in agreement, but for octahedral are much lower. Also, for Fe^{3+} site, the average isomer shift obtained by us agrees with the value fixed by Dunlap et al. [54], but the quadrupole splitting is in the limit of the distribution imposed by those authors. The Fe^{3+}/Fe^{2+} ratio is higher in our study, but consistent with expected values. As for Muong Nong samples, the ratio is higher than for the other tektites. In the analysis of Dunlap et al. [54], this ratio for australite tektites is close to Muong Nong, and for Tibetanite is higher. The differences, well observed in these charts, are related to the method of analysis. Our results are comparable with ratios obtained with many wet chemical analyses, as also referred by Dunlap et al. [54] when explaining the results obtained with their fitting method. Fudali et al. [61] used four wet chemical analysis (two standard volumetric methods, an experimental volumetric method for direct determination of Fe^{3+} and a colorimetric method) and two instrumental techniques (Mössbauer spectroscopy and electron spin resonance). They found out that the Fe^{3+}/Fe^{2+} ratios are in the range 0.02–0.12 and agree with what they believe is the best published analysis for tektites (review [62]). We obtained Fe^{3+}/Fe^{2+} ratios within these

values, except for Muong Nong tektites, which was to be expected given that they are supposedly found nearest to the original impact crater [19].

There seems to be no doubt that moldavites are analogous to Australasian tektites: they almost always plot closely grouped together on Figure 22. The exception is the Fe^{2+} octagonal coordination IS x QS chart (Figure 22b).

The cambodiatite sample is mostly individualized, plotting only once near the vietnamite (Figure 22a).

Our tibetanite sample sometimes plots not far from australasites (near the vietnamite on Figure 22b and near the thailandite in Figure 22d) but we must note the low QS for Fe^{3+} (0.01 mm/s on Figure 22c) and some individuation on Figure 22a. Our analyses do not conclusively remove persistent doubts that tibetanites are fake Australasian tektites (see, e.g., https://bit.ly/3s62aAe (accessed on 10 June 2021)).

Laotian Muong-Nong samples (MN1 and MN2) always plot far from each other but their high Fe^{3+} contents (between 13% and 15%) allows them to display a linear trend with the Chinese Muong-Nong (16.5% Fe^{3+}) on Figure 22d. There are evidences that Muong Nong tektites may have a higher Fe^{3+}/Fe^{2+} ratio than splash form tektites, consistent with their general morphology and solidification from the melt at a lower temperature [19].

The Darwin Glass stands, in overall, separate among the other items, namely in Figure 22d, so Mössbauer spectroscopy is also useful to distinguish Darwin Glasses from tektites.

4. Conclusions

X-ray diffractograms evidence only kamacite in the interior of both iron meteorites and weathering oxides on their crust (fusion and terrestrial weathering). Mössbauer spectra confirm these results.

In Campo del Cielo meteorite, Widmanstätten patterns and schreibersite inclusions are evident. The unregistered iron meteorite exhibits Neumann lines along with schreibersite inclusions. Campo del Cielo meteorite is found to be an octahedrite and the Find 1 iron meteorite a hexahedrite. This general classification for this unregistered meteorite shall be further refined, namely when we have Ge, Ga and Ir analyses.

The composition of the unregistered NWA 1990 stony meteorite is common to high-Si stony meteorites. XRD patterns show several silicate minerals, but iron is not included on them, as evidenced by Mössbauer spectroscopy at 4.2 K. At this temperature, maghemite and a very small amount of FeS are found. These results, together with minerals content, suggest that NWA 1990 stony meteorite is an enstatite achondrite.

Mössbauer spectroscopy is one of the most powerful methods for determination of the iron atoms valence/spin state and coordination and its importance for the characterization of both meteorites and tektites cannot be overstated.

The observed hyperfine parameters and higher Fe^{3+}/Fe^{2+} ratios in Muong Nong than in other tektites are consistent with the conditions under which Muong Nong tektites are assumed to be formed.

The analyses of a Darwin Glass by Mössbauer spectroscopy is consistent with the formation of this impact glass and reinforces the idea of the use of Mössbauer spectroscopy to distinguish between tektites and impactites.

Author Contributions: Conceptualization, B.F.O.C., E.I.A.; methodology, B.F.O.C., E.I.A., A.C.B., analysis: B.F.O.C., P.A.O.C.S., A.C.B.; writing. B.F.O.C., E.I.A.; funding acquisition, B.F.O.C., E.I.A., A.C.B. All authors have read and agreed to the published version of the manuscript.

Data Availability Statement: The data presented in this study are contained within this article.

Conflicts of Interest: The authors declare no conflict of interest.

References

1. Burke, J.G. *Cosmic Debris: Meteorites in History*; University of California Press: Berkeley, CA, USA, 1986.
2. Dennison, J.E.; Lingner, D.W.; Lipschutz, M.E. Antarctic and non-Antarctic meteorites form different populations. *Nature* **1986**, *319*, 390–393. [CrossRef]
3. Varela, M.E.; Kurat, G. Glasses in meteorites and the primary liquid condensation model. *Mitt. der Osterreichischen Mineral. Ges.* **2009**, *155*, 279–320.
4. Cannon, K.M.; Mustard, J.F. Preserved glass-rich impactites on Mars. *Geology* **2015**, *43*, 635–638. [CrossRef]
5. French, B.M. *Traces of Catastrophe: A Handbook of Shock-Metamorphic Effects in Terrestrial Meteorite Impact Structures*; Lunar and Planetary Institute: Houston, TX, USA, 1998.
6. Koeberl, C. Tektite origin by hypervelocity asteroidal or cometary impact. *Large Meteor. Impacts Planet. Evol.* **1994**, *293*, 133.
7. O'Keefe, J.A. *Tektites and Their Origin*; Elsevier: New York, NY, USA, 1976.
8. Howard, K.T. Physical distribution trends in Darwin glass. *Meteorit. Sci.* **2009**, *44*, 115–129. [CrossRef]
9. Chapman, D.R.; Keil, K.; Annell, C. Comparison of Macedon and Darwin glass. *Geochim. Cosmochim. Acta* **1967**, *31*, 1595–1603. [CrossRef]
10. Dunlap, R.A. An investigation of Fe oxidation states and site distributions in a Tibetan tektite. *Hyperfine Interact.* **1997**, *110*, 217. [CrossRef]
11. Devouard, B.; Rochette, P.; Gattaccec, J.; Barrat, J.-A.; Moustard, F.; Valenzuela, E.M.; Alard, O.; Balestrieri, M.L.; Bigazzi, G.; Dos Santos, E.; et al. A new tektite strewnfield in Atacama, Chile. *LPI* **2014**, *77*, 5394.
12. Rochette, P.; Bezaeva, N.S.; Kosterov, A.; Gattacceca, J.; Masaitis, V.L.; Badyukov, D.D.; Giuli, G.; Lepore, G.O.; Beck, P. Magnetic properties and redox state of impact glasses: A review and new case studies from Siberia. *Geosciences* **2019**, *9*, 225–249. [CrossRef]
13. Povenmire, H.; Cornec, J.H. The 2014 Report on the Belize tektite strewn field. *LPI* **2015**, *1832*, 1132.
14. McCall, G.J.M. *Tektites in the Geological Record: Showers of Glass from the Sky*; The Geological Society: London, UK, 2001.
15. Koeber, C. Geochemistry and origin of Muong Nong-type tektites. *Geochim. Cosmochim. Acta* **1992**, *56*, 1033–1064. [CrossRef]
16. Thorpe, A.N.; Senftl, F.E.; May, L.; Barkatt, A.; Adel-Hadadi, M.A.; Marbury, G.S.; Izett, G.A.; Maurrasse, F.R. Comparison of the magnetic properties and Mössbauer analysis of glass from the Cretaceous-Tertiary boundary, Beloc, Haiti, with tektites. *J. Geophys. Res. Planets* **1994**, *99*, 10881–10886. [CrossRef]
17. Oskarsson, N.; Helgason, O.; Sigurdsson, H. Oxidation state of iron in tektite glasses from the Cretaceous/Tertiary boundary. In *New Developments Regarding the KT Event and Other Catastrophes in Earth History*; Ryder, G., Fastovsky, D., Gartner, S., Eds.; Geological Society of America Special Paper: Boulder, CO, USA, 1996; Volume 307, pp. 445–452.
18. Howar, K.T. Volatile enhancement dispersal of high velocity impact melts and the origin of tektites. *Proc. Geol. Ass.* **2011**, *122*, 363–382. [CrossRef]
19. Son, T.H.; Koeberl, C. Chemical variation within fragments of Australasian tektites. *Met. Planet. Sci.* **2005**, *46*, 805–815. [CrossRef]
20. Cabanillas, E.D.; Palacios, T.A. An hexahedrite meteorite from Campo del Cielo Fall. *Planet. Space Sci.* **2006**, *54*, 303–309. [CrossRef]
21. Villar, L.M. La dispersion meteorica en la Argentina y Chile. In *Ciencia e Investigacion Organo de informacion del CONICET.*; CONKICET: Buenos Aires, Argentina, 1968; pp. 302–314.
22. Ferreira, L.M.G.; Alves, E.I.; Gonçalves, M.; Costa, B.F.O. North West Africa stony meteorite: A case study. *Hyperfine Interact.* **2020**, *241*, 1–6. [CrossRef]
23. Costa, B.F.O.; Klingelhöfer, G.; Alves, E.I. 57Fe Mössbauer spectroscopy studies of tektites from Khon Kaen, NE Thailand. *Hyperfine Interact.* **2014**, *224*, 51–56. [CrossRef]
24. Costa, B.F.O.; Klingelhöfer, G.; Panthöfer, M.; Alves, E.I. Backscattering Mössbauer MIMOS II and XRF studies on tektites from different strewn fields. *Hyperfine Interac.* **2014**, *226*, 613–619. [CrossRef]
25. Goldstein, J.I.; Scott, E.R.D.; Chabot, N.L. Iron meteorites: Crystallization, thermal history, parent bodies, and origin. *Geochemistry* **2009**, *69*, 293–325. [CrossRef]
26. Klingelhöfer, G.; Morris, R.; Bernhardt, B.; Rodionov, D.; Souza, P.D.; Squyres, S.; Foh, J.; Kankeleit, E.; Bonnes, U.; Gellert, R. Athena MIMOS II Mössbauer spectrometer investigation. *J. Geophys. Res.* **2003**, *108*, 8067. [CrossRef]
27. Scorzelli, R.B.; Danon, J.; Galvão da Silva, E. Solid state transformations in Fe-Ni alloys from meteorites in powder form. *Hyperfine Interact.* **1986**, *28*, 979–983. [CrossRef]
28. Hammant, O.M.; Forder, S.D.; Bingham, P.A.; Hand, R.J. Structural studies of iron in vitrified toxic wastes. *Hyperfine Interact.* **2009**, *192*, 37–42. [CrossRef]
29. Forder, S.D.; Hammant, O.M.; Bingham, P.A.; Hand, R.J. Concerning the use of standards for identifying coordination environments in glasses. *J. Phys. Conf. Ser.* **2010**, *217*, 012072. [CrossRef]
30. Silva, P.C.; Guerra, M.; Marques, R.; Prudencio, M.I.; Ramalho, A.; Khomchenko, V.A.; Klingelhoefer, G.; Alves, E.I.; Batista, A.C.; Costa, B.F.O. Characterization of an iron meteorite using 57Fe Mössbauer spectroscopy and elemental analysis. In Proceedings of the XXXIX Colloquium Spectroscopicum Internationale, Figueira da Foz, Portugal, 30 August–3 September 2015; p. 240.
31. Costa, B.F.O.; Silva, P.C.; Klingelhoefer, G.; Alves, E.I. Characterization of two different iron meteorites. In Proceedings of the International Conference on the Applications of the Mössbauer Effect 2015, Hamburg, Germany, 13–18 September 2015; p. 297.
32. Silva, P.C. An Iron-Nickel Meteorite Characterization Using Different Experimental Techniques. Master's Thesis, University of Coimbra, Coimbra, Portugal, 2015.

33. Dos Santos, E.; Gattacceca, J.; Rochette PScorzelli, R.B.; Fillion, G. Magnetic hysteresis properties and 57Fe Mössbauer spectroscopy of iron and stony-iron meteorites: Implications for mineralogy and thermal history. *Phys. Earth Plan Inter.* **2015**, *2–12*, 30–64. [CrossRef]

34. Oshtrakh, M.I.; Grokhovsky, V.I.; Abramova, N.V.; Semionkin, V.A.; Milde, O.B. Iron-nickel alloy from iron meteorite Chinga studied by Mössbauer spectroscopy with high velocity resolution. *Hyperfine Interact.* **2009**, *190*, 135–142. [CrossRef]

35. Goryunov, M.V.; Yakovlev, G.A.; Chukin, A.V.; Grokhovsky, V.I.; Semionkin, V.A.; Oshtrakh, M.I. Iron meteorites and their weathering products: High velocity resolution Mössbauer spectroscopy of the iron-bearing minerals. *Eur. J. Miner.* **2016**, *28*, 601–610. [CrossRef]

36. Scorzelli, R.B.; Dos Santos, E. Meteoritic Fe-Ni alloys: A review of 57Fe Mössbauer spectroscopy studies. *Geochemistry.* **2019**, *79*, 125547. [CrossRef]

37. Yang, J.; Goldstein, J.I.; Scott, E.R.D.; Michael, J.R.; Kotula, P.G.; Pham, T.; McCoy, T.J. Thermal and impact histories of reheated group IVA, IVB, and ungrouped iron meteorites and their parent asteroids. *Meteorit. Planet. Sci.* **2011**, *46*, 1227–1252. [CrossRef]

38. Fleischer, I.; Schroeder, C.; Klingelhoefer, G.; Zipfel, J.; Morris, R.V.; Ashley, J.W.; Gellert, R.; Wehrheim, S.; Ebert, S. New insights into the mineralogy and weathering of the Meridiani Planum meteorite, Mars. *Meteor. Plan. Sci.* **2011**, *46*, 21–34. [CrossRef]

39. Scot, E.R.; Wasso, J.T. Classification and properties of iron meteorites. *Rev. Geophys.* **1975**, *13*, 527–546. [CrossRef]

40. Oshtrakh, M.I.; Larionov MYu Grokhovsky, V.I.; Semionkin, V.A. Study of iron meteorite Sikhote-Alin and extracted iron-nickel phosphides using Mössbauer spectroscopy with high velocity resolution. *Hyperfine Interact.* **2008**, *186*, 53–59. [CrossRef]

41. Oshtrakh, M.I.; Larionov MYu Grokhovsky, V.I.; Semionkin, V.A. An analysis of Fe and Ni distribution in M1, M2 and M3 sites of iron-nickel phosphides extracted from Sikhote-Alin meteorite using Mössbauer spectroscopy with a high velocity resolution. *J. Mol. Struct.* **2011**, *993*, 38–42. [CrossRef]

42. Oshtrakh, M.I.; Larionov MYu Grokhovsky, V.I.; Semionkin, V.A. Study of rhabdite (iron nickel phosphide) microcrystals extracted from Sikhote-Alin iron meteorite by magnetization measurements and Mössbauer spectroscopy. *Mat. Chem. Phys.* **2011**, *130*, 373–380. [CrossRef]

43. Oshtrakh, M.I.; Larionov MYu Grokhovsky, V.I.; Semionkin, V.A. Temperature dependent high velocity resolution Mössbauer spectroscopic study of iron nickel phosphide microcrystals (rhabdites) extracted from Sikhole-Alin iron meteorite. *J. Alloys Comp.* **2011**, *509*, 1781–1784. [CrossRef]

44. de Bakker, P.M.A.; de Grave, E.; Vandenberghe, R.E.; Bowen, L.H. Mössbauer study of small-particle maghemite. *Hyperfine Interact.* **1990**, *54*, 493–498. [CrossRef]

45. Cuda, J.; Kohout, T.; Tucek, J.; Filip, J.; Medrik, I.; Mashlan, M.; Zboril, R. Mössbauer study and magnetic measurement of troilite extract from Natan iron meteorite. *AIP Conf. Proc.* **2012**, *1489*, 145–154.

46. Munayco, P.; Munayco, J.; Valenzuela, M.; Rochette, P.; Gattacceca, J.; Scorzelli, R.B. 57Mössbauer spectroscopy studies of chondritic meteorites from the Atacama Desert, Chile: Implications for weathering processes. *Hyperfine Interact.* **2014**, *224*, 257–262. [CrossRef]

47. Bland, P.A.; Sexton, A.S.; Jull, A.J.T.; Bevan, A.W.R.; Berry, F.J.; Thornley, D.M.; Astin, T.R.; Britt, D.T.; Pillinger, C.T. Climate and rock weathering: A study of terrestrial age dated ordinary chondritic meteorites from hot desert regions. *Geochim. Cosmochim. Acta* **1998**, *62*, 3169–3184. [CrossRef]

48. Bogusz, P.; Galazka-Friedman, J.; Brzozka, K.; Jakubowska, M.; Wozniak, M.; Karwowski, L.; Duda, P. Mössbauer spectroscopy as a useful method for distinguishing between real and false meteorites. *Hyperfine Interact.* **2019**, *240*, 126. [CrossRef]

49. Hsu, W. Geochemical and petrographic studies of oldhamite, diopside and roedderite in enstatite meteorites. *Meteorit. Planet. Sci.* **1998**, *33*, 291–301. [CrossRef]

50. Keil, K. Enstatite achondrite meteorites (aubrites) and the histories of their asteroidal parent bodie. *Chemie Erde* **2010**, *70*, 295–317. [CrossRef]

51. Mineralogy of Aubrite meteorite. Available online: https://www.mindat.org/min-49873.html (accessed on 10 June 2021).

52. Dunlap, R.A. A Mössbauer Effect investigation of the enstatite chondrite from Abee, Canada. *Hyperfine Interact.* **1997**, *110*, 209–215. [CrossRef]

53. Maliszewski, A.; Szlachta, K.; Galazka-Friedman, J.; Bakun-Czubarow, N. Mössbauer studies of Polish enstatite meteorite-Zaklodzie. *Hyperfine Interact.* **2008**, *186*, 121–125. [CrossRef]

54. Dunlap, R.A.; Sibley, A.D.E. A Mössbauer effect study of Fe-site occupancy in Australasian tektites. *J. Non Cryst. Solids* **2004**, *227*, 36–41. [CrossRef]

55. Ceron Loayza, M.L.; Bravo Cabrejo, J.A. Characterization of magnetic iron phases in impactites by Mössbauer spectroscopy. *Hyperfine Interact.* **2019**, *240*. [CrossRef]

56. Verma, H.C.; Misra, S.; Shyam Prasad, M.; Bijlani, N.; Tripathi, A.; Newsom, H. Mössbauer studies on impactites from Lonar impact crater. *Hyperfine Interact.* **2008**, *186*, 15–22. [CrossRef]

57. Bustamante, A.; Espinoza, S.; Morales, G.; Scorzelli, R.B. Mössbauer studies of impactites from Huamalies province in Huanuco Regio. *Hyperfine Interact.* **2005**, *166*, 14.

58. Rossano, S.; Balan, E.; Morin, G.; Bauer, J.-P.; Calas, G.; Brouder, C. Fe-57 Mössbauer spectroscopy of tektites. *Phys. Chem. Miner.* **1999**, *26*, 530–538. [CrossRef]

59. Dunlap, R.A.; Eelman, D.A.; MacKay, G.R. A Mössbauer effect investigation of correlated hyperfine parameters in natural glasses (tektites). *J. Non Cryst. Solids* **1998**, *223*, 141–146. [CrossRef]

60. Dunlap, R.A.; McGraw, J.D. A Mössbauer effect study of Fe environments in impact glasses. *J. Non Cryst. Solids* **2007**, *353*, 2201–2205. [CrossRef]
61. Fudali, R.F.; Dyar, M.D.; Griscom, D.L. Schreiber. The oxidation state of iron in tektite glass. *Geochim. Cosmochim. Acta* **1987**, *51*, 2749–2756. [CrossRef]
62. Lukanin, O.A.; Kadik, A.A. Decompression mechanism of ferric iron reduction in tektite melts during their formation in the impact processes. *Geochem. Int.* **2007**, *45*, 857–881.